Biomaterials 225 (2019) 119517

Contents lists available at ScienceDirect

Biomaterials

journal homepage: www.elsevier.com/locate/biomaterials

3D bioengineered tissue model of the large intestine to study inflammatory bowel disease

Terrence T. Roh, Ying Chen, Harry T. Paul, Chengchen Guo, David L. Kaplan*

Tufts University, Department of Biomedical Engineering, 4 Colby St. Medford, MA, 02155, USA

ARTICLE INFO

Keywords:
Tissue engineering
Intestine tissue
Inflammatory bowel disease
Intestinal immune system
Colonoids
Monocyte-derived macrophages
silk

ABSTRACT

An *in vitro* model of intestinal epithelium with an immune component was bioengineered to mimic immunologic responses seen in inflammatory bowel disease. While intestinal immune phenomena can be modeled in transwells and 2D culture systems, 3D tissue models improve physiological relevance by providing a 3D substrate which enable migration of macrophages towards the epithelium. An intestinal epithelial layer comprised of non-transformed human colon organoid cells and a subepithelial layer laden with monocyte-derived macrophages was bioengineered to mimic native intestinal mucosa cell organization using spongy biomaterial scaffolds. Confluent monolayers with microvilli, a mucus layer, and infiltration of macrophages to the basal side of the epithelium were observed. Inflammation, induced by *E. coli* O111:B4 lipopolysaccharide and interferon γ resulted in morphological changes to the epithelium, resulting in ball-like structures, decreased epithelial coverage, and increased migration of macrophages to the epithelium. Analysis of cytokines present in the inflamed tissue model demonstrated significantly upregulated secretion of pro-inflammatory cytokines that are often associated with active inflammatory bowel disease, including CXCL10, IL-1β, IL-6, MCP-2, and MIP-1β. The macrophage layer enhanced epithelial and biochemical responses to inflammatory insult, and this new tissue system may be useful to study and develop potential therapies for inflammatory bowel disease.

1. Introduction

The intestine presents a surface area of 250 m^3–400 m^3 to an external environment which comprises of digesting food and a population of 10^{13}–10^{14} bacteria known as the gut microbiota [1,2]. A single layer of the intestinal epithelium ensures that these microorganisms do not invade into the host with coordination from the intestinal immune system which both directly eliminates pathogens and secretes factors contributing to epithelial renewal and remodeling [3–5]. Dysregulation of the intestinal immune system can result in inflammatory bowel disease (IBD) in which the intestinal immune system becomes hyperactive and causes unnecessary inflammation in the intestinal mucosa [5]. Intestinal macrophages are one of the largest populations of macrophages in the body and are primarily concentrated directly underneath the single layer of epithelium, acting as the first line of defense [6–8]. This strategic subepithelial localization allows for recognition and phagocytosis of invading pathogens within minutes and modulation of bacterial populations in the microbiota [7,9]. Moreover, intestinal macrophages secrete factors promoting epithelial cell renewal including Wnt signaling molecules and hepatocyte growth factor [10,11].

Investigations of intestinal immune phenomena are often conducted using *in vitro* cell or tissue models or *in vivo* mice models. Though *in vitro* 2D models include immune cell co-cultures with epithelial cells, many use cell-line based epithelial modeling [12–14]. A recently published *in vitro* 3D model of inflammatory bowel disease used Caco-2 and HT29-MTX intestinal epithelial cell lines, but does not include contributions of the immune system in epithelial barrier pathologies [15]. Mice models present an alternative for intestinal epithelial-immune studies. For example, macrophage ablation in mice reduced levels of Leucine Rich Repeat Containing G Protein-Coupled Receptor 5 positive (LGR5+) intestinal stem cells, disrupted development of M cells, and enhanced goblet cell density [16]. This work demonstrates important functions of macrophages in the intestinal epithelium; however, the study was carried out in mice and the relevance to human physiology is unclear. In the present study, we utilized an *in vitro* 3D tissue engineered system which models colonic epithelium-immune responses using human LGR5+ colonic organoids (colonoids) to better mimic physiologic responses of the human intestinal epithelium. Furthermore, we utilized co-cultures with human primary monocyte-derived macrophages layered underneath the epithelial layer, mimicking intestinal tissue organization. Non-transformed human cells were used to improve

* Corresponding author.
E-mail address: david.kaplan@tufts.edu (D.L. Kaplan).

https://doi.org/10.1016/j.biomaterials.2019.119517
Received 16 September 2019; Accepted 21 September 2019
Available online 25 September 2019
0142-9612/

relevance vs the more commonly used cell-line-based cultures.

To ensure physiologic responses of the intestinal epithelium, human colonoids were cultivated. Colonoids are untransformed LGR5 + epithelial stem cells derived from colonic crypts, are capable of indefinite propagation, and can differentiate towards all epithelial lineages [17]. Under inflammatory conditions, intestinal epithelial cells direct immune cell responses against pathogens and experience impaired proliferation resulting in a loss of intestinal epithelial coverage [18–20]. In a previous study examining the expression of inflammation-associated genes between intestinal epithelia derived from cell-lines, human primary cells, and intestinal organoids in a 3D system, organoids were shown to be the most sensitive to inflammation cues [21]. Moreover, colonoids were used to model epithelial-immune interactions as opposed to small intestine organoids, due to the colonic lamina propria containing a relatively higher population of macrophages than in the small intestine lamina propria [3].

A cylindrical scaffold shape was used due to previous intestinal modeling showing that intestinal epithelia arranged in a tubular configuration results in low oxygen tensions within the lumen, enabling the growth of anaerobic bacteria [21,22]. Moreover, the physiology of the intestine is tubular and the cylindrical design of the model mimics intestine architecture. To achieve the 3D intestinal tissue organization, we modified our previous small intestine epithelium tissue model cultured on lyophilized silk protein sponge matrices by introducing the modular secondary macrophage laden 3D tissue layer [21–23]. The double cylindrical scaffold is a critical feature, enabling replacement of the macrophage-laden outer layer without disruption of the inner scaffold layer containing the epithelium and the observation of macrophage migration towards the epithelial layer. While intestinal macrophages are constantly replenished by bone marrow derived monocytes from peripheral blood, 3D tissue engineered constructs with immune cells are typically cultured to a terminal timepoint and are not able to replenish immune cell populations [24–27]. The current tissue model is a significant advance in both biomaterial and biology over the previously published system.

During active IBD, monocytes massively infiltrate the epithelium and elevate levels of proinflammatory cytokines including interleukins 1β and 6 (IL-1β & IL-6), monocyte chemoattractant proteins 1 and 2 (MCP-1 & MCP-2), and macrophage inflammatory protein 1β (MIP-1β/CCL4) are detected [28–31]. This 3D silk scaffold system presents substrates for cultivation and movement of macrophages towards the colonic epithelial layer allowing for evaluation of inflammation *in vitro*. The silk sponges show formation of a porous film for the cultivation of an epithelial layer with appropriate material properties for intestinal tissue engineering. Analysis of the epithelium of inflamed 3D colonoid-epithelial co-cultures showed significant decreases in epithelial coverage and morphology in addition to the infiltration of macrophages towards the basal side of the epithelium. Cytokine analysis showed enhanced secretion of inflammatory cytokines mimicking cytokine profiles found *in vivo* in response to inflammation. This paper presents a novel system using human colonoids and human primary monocyte-derived macrophages cultured in a 3D sponge format with epithelial-immune interactions reflective of IBD.

2. Materials

2.1. Cell culture

Human colonoid culture – Human colonoids isolated from the large intestine epithelium were provided by Dr. Mary Estes from Baylor College of Medicine under approved protocols. Colonoids were cultured in 24 well tissue culture plates in Matrigel (Corning Inc, Corning, NY) droplet cultures based on previously described protocols [32]. Frozen vials of colonoids were thawed and suspended in Matrigel and plated in 10 μL droplets with 3 droplets in each well. Each well of colonoids received 500 μL of high Wingless/Integrated (Wnt) media and was replaced every other day. High Wnt media consists of 75% Wnt-3A conditioned media harvested from L Wnt-3A cells (American Type Culture Collection, Manassas, VA), 10% R-spondin conditioned media harvested from R-spondin generating cells (courtesy of Dr. Calvin Kuo, Palo Alto, CA), 5% Noggin conditioned media harvested from Noggin generating cells (courtesy of Dr. Gijs van den Brink, Amsterdam, Netherlands), and 10% complete media without growth factors (CMGF- media) and growth factors. CMGF- media consists of Advanced Dulbecco's Modified Eagle Medium (DMEM)/Ham's F-12 (ThermoFisher Scientific, Waltham, MA) supplemented with 1x GlutaMAX (ThermoFisher), 1x Penicillin-Streptomycin (ThermoFisher), and 10 mM HEPES buffer (ThermoFisher). Final concentrations of growth factors in the high Wnt media are 0.5x B-27 supplement (ThermoFisher), 0.5x N-2 supplement (ThermoFisher), 0.5 mM N-Acetyl-L-cysteine (Sigma-Aldrich, St. Louis, MO), 25 ng/mL mouse recombinant epidermal growth factor (ThermoFisher), 250 nM A-83-01 (Tocris Bioscience, Bristol, United Kingdom), 5 mM SB 202190 (Sigma-Aldrich), 5 mM nicotinamide (Sigma-Aldrich), 5 nM [15-Leucine]-Gastrin I (Sigma-Aldrich), and 100 μg/mL Primocin (Invivogen, San Diego, CA).

Human monocyte-derived macrophage culture – Monocytes were isolated using the Pan Monocyte Isolation Kit (Miltenyi Biotec Inc, Bergisch Gladbach, Germany) per manufacturer's instructions from unpurified buffy coats (Research Blood Components LLC, Boston, MA). Isolated monocytes were frozen in 10% DMSO (Sigma-Aldrich) and 90% in macrophage media consisting of RPMI 1640 medium with 10% heat inactivated FBS (ThermoFisher), 10 mM HEPES (ThermoFisher), 1 mM sodium pyruvate (ThermoFisher), 0.05 mM 2-mercaptoethanol (ThermoFisher), and 1X Penicillin-Streptomycin (ThermoFisher). Monocytes were thawed as needed and differentiated into macrophages by culturing in 50 ng/mL macrophage colony-stimulating factor (ThermoFisher) supplemented macrophage media for 6 days with media changes every other day. For M1 polarization, monocyte-derived macrophages were then cultured in macrophage media with 100 ng/mL lipopolysaccharides (LPS) from *E. coli* O111:B4 (Sigma-Aldrich) and recombinant human interferon γ (IFNγ) (PeproTech, Rocky Hill, NJ).

2.2. Silk scaffolds

Silk fibroin (hereafter referred to as silk) extracted from *Bombyx mori* silkworm cocoons was processed to a 5–7% (wt/vol) silk solution following established protocols [33]. Hollow channels were formed in silk scaffolds using a cylindrical mold cast comprised of polydimethylsiloxane (Dow Corning, Midland, MI) following previous protocols [22]. A 2 mm diameter Teflon-coated stainless-steel wire (McMaster-Carr, Elmhurst, IL) was inserted through the cross section of the cylindrical mold to form the channel. The silk solution was then poured into the molds and frozen overnight at −20 °C. The frozen silk was then placed in a lyophilizer for freeze-drying. Once fully dried, the silk scaffolds were autoclaved to induce β-sheet conformation, stabilizing the scaffold structure and preventing solubilization. The scaffolds were then soaked in distilled water overnight and cut into silk sections with 8 mm long hollow channels. A 6 mm biopsy punch (Acuderm Inc, Fort Lauderdale, FL) was used to punch out an inner silk scaffolds with a diameter of 6 mm, a 2 mm diameter hollow center and length of 8 mm. A 10 mm biopsy punch (Acuderm Inc) was then used to punch out a 10 mm diameter outer scaffold with a 6 mm diameter hollow center and length of 8 mm.

2.3. Cell seeding

Inner scaffolds – Human colonoids were seeded on the inner surface of the 2 mm diameter hollow channels following previously described protocols for human intestinal organoids [21]. For each scaffold, 500 μl of collagen gel was added into the spongy silk scaffold and gelled at 37 °C for 45 min. The collagen gel was 80% 2.01 mg/ml rat tail collagen type I (First Link Ltd, Wolverhampton, United Kingdom), 10% 10X

DMEM (Sigma-Aldrich), and 10% CMGF- media. 5 M NaOH was used to neutralize the collagen gel. Two wells of confluent colonoids were dissociated and seeded following a previously established protocol e. In short, Matrigel droplets containing confluent colonoids were suspended in 500 μL/well of 4 °C 0.5 mM ethylenediamine tetraacetic acid (ThermoFisher) and centrifuged at 200 g at 4 °C for 5 min. The resultant cell pellet was then digested with 0.05% Trypsin-EDTA (ThermoFisher) for 4 min at 37 °C. The trypsin was inhibited with CMGF- media containing 10% fetal bovine serum (ThermoFisher) and the colonoid pellet was further dissociated via pipetting. The resulting cell suspension was passed through a 40 μm cell strainer (Corning) and centrifuged again at 1500 rpm for 5 min to obtain a cell pellet. The pellet was resuspended in 30 μL of high Wnt media supplemented with 10 μM Y-27632 (Sigma-Aldrich) and pipetted onto one side of the hollow channel of the scaffold. The scaffolds were transferred to 37 °C for 45 min. The scaffold was then flipped 180° and another 30 μL of colonoid suspension made from another 2 wells of confluent colonoids was pipetted into the hollow channel to completely coat the inner surface of the channel. The inner scaffolds were then cultured in high Wnt media with 10 μM Y-27632 for 1 day before being cultured in high Wnt media for a total of 7 days. Media changes occurred every other day. Seeded colonoids were differentiated by culturing in differentiation medium comprised of 90% CMGF- supplemented with 10% R-spondin conditioned media, 1x B-27 supplement, 1x N-2 supplement, 1 mM N-Acetyl-L-cysteine, 50 ng/mL mouse recombinant epidermal growth factor, 500 nM A-83-01, 10 nM [15-Leucine]-Gastrin I, and 100 μg/mL Primocin.

Outer scaffolds – Monocytes suspended in collagen gel (80% 2.01 mg/ml rat tail collagen type I (First Link Ltd), 10% 10X DMEM (Sigma-Aldrich), and 10% macrophage media) were seeded throughout the bulk of the outer scaffold at 3×10^6 cells/scaffold. Seeded monocytes were differentiated to uncommitted macrophages (M0) by 6 days of culture in macrophage media supplemented with 50 ng/mL MCSF. The outer scaffold was then either cultured for 1 day in macrophage media with 100 ng/mL LPS and 20 ng/mL IFNγ for M1 polarization or in plain macrophage media. The outer scaffold was combined with the inner scaffold on day 8 as shown in Fig. 2D. Once combined M1 differentiation was maintained by 100 ng/mL LPS and 20 ng/mL IFNγ in the co-culture media.

2.4. Scanning electron microscopy

Samples were fixed in 1% glutaraldehyde (Sigma-Aldrich) for 1 h and then rinsed in PBS and then deionized water. After the rinses, the sample was dehydrated in a graded series of ethanol (30%, 50%, 70%, 90%, 100%) before being dehydrated overnight in 100% ethanol. The samples were dried via critical point drying using a liquid CO_2 dryer (Tousimis 931GL, Tousimis Research Corp.). Samples were then coated with a 10 nm thick layer of Pt/Pd using a sputter coater (EMS 150T S Metal Sputter Coater, Electron Microscopy Sciences). Samples were imaged on a scanning electron microscope (Zeiss UltraPlus SEM or Zeiss Supra 55 VP SEM, Carl Zeiss SMT Inc.) at 2–3 kV.

2.5. Mechanical characterization of scaffolds

The mechanical properties of silk sponges were characterized using an Instron 3366 (Instron Inc.). The outer sponges have an outer dimeter of 10 mm, an inner diameter of 6 mm, and a length of 8 mm. The inner sponges have an outer diameter of 6 mm, an inner diameter of 2 mm, and a length of 8 mm. The compression tests were done on individual inner and outer sponges along the longitudinal direction. In each test, the hydrated samples were loaded onto the testing frame at room temperature and then were compressed with a rate of 2.0 mm/min. Compressive modulus were calculated at 5% strains for comparison. At least n = 3 samples were used to calculate average modulus with standard deviation.

2.6. Immunofluorescence and epithelium measurements

Seeded 3D silk scaffolds and transwell membranes were fixed in 4% paraformaldehyde (Santa Cruz Biotechnology Inc, Dallas, TX). For luminal surface imaging, inner scaffolds were cut along the hollow channel to expose the colonoid seeded lumen surface to blocking solutions and antibodies. To obtain transverse sections of the model, fixed samples were suspended in an increasing gradient of sucrose (Sigma) and optimal cutting temperature (OCT) compound (VWR, Radnor, PA) over 4 days. Scaffolds were then embedded in OCT and sectioned at 20 μm thickness. All samples were permeabilized and blocked with 5% bovine serum albumin (Sigma Aldrich) and 0.1% Triton X-100 (Fisher Scientific, Hampton, NH) in phosphate-buffered saline (PBS, Thermofisher) for 30 min. Samples were incubated overnight at 4 °C in PBS with human e-cadherin antibody (1:250, ab1416) (Abcam, Cambridge, United Kingdom), human mucin-2 antibody (1:50, H-300) (Santa Cruz Biotechnology Inc), human CD-68 antibody (1:200, ab955), and human iNOS antibody (1:150, ab15327). The samples were rinsed with PBS then incubated in goat anti-mouse Alexa Fluor 488 (1:250, A28175) (Thermofisher) or goat anti-rabbit Alexa Fluor 546 (1:1000, A-11010) (Thermofisher). Scaffolds were counterstained with 4',6-diamidino-2-phenylindole, dihydrochloride (DAPI) (Thermofisher). A Leica SP8 confocal microscope (Leica Microsystems, Wetzlar, Germany) with z-series capability was used to image samples. Scaffolds were observed under preset filters for DAPI (Ex/Em: 359/461 nm), AF488 (Ex/Em: 499/520) and AF546 (556/573). Leica Application Suite X (Leica Microsystems) ver 3.5.2.18963 was used to assemble confocal maximum projection images. ImageJ with the Fiji plugin was used to measure epithelial coverage and epithelial heights on histologic sections of the models. Epithelial height was measured at every 5 μm where epithelium was undisrupted.

2.7. Cytokine array

Cytokines were measured by chemiluminescence using commercial arrays (RayBiotech Inc, Norcross, GA) following manufacturer's instructions. Media was collected at days 3 of differentiation media culture. Blot intensities were measured using BD ChemiDoc Imaging System (Becton, Dickinson and Company, Franklin Lakes, NJ) and blot intensities were all normalized to each other using ImageJ. Principle component analysis and biplots were calculated using Matlab R2018b.

2.8. Mucus thickness measurements

Transverse sections of the inner scaffold were obtained using the sucrose-OCT gradient equilibration and cryo-embedding procedure outlined for immunofluorescence. 20 μm slices were obtained and rinsed with tap water for 2 min. The slides were then dried for 20 min and rinsed with 3% acetic acid (pH 2.5) for 2 min and stained in Alcian blue (Sigma) for 15 min. The samples were then rinsed in running tap water for 5 min and dipped in deionized water once. The slides were dehydrated through an alcohol series, cleared in xylene and coverslipped using DPX Mountant (Sigma). A light microscope was used to evaluate stained samples. Mucus thickness measurements were taken every 5 μm where the epithelium remained intact using ImageJ with the Fiji plugin.

2.9. Statistical analysis

Statistical significances were calculated using Analysis of Variance (ANOVA) paired with Tukey's post-hoc test using Minitab 18 (Minitab LLC, State College, PA). Data were reported as mean ± standard deviation. P-values ≤ 0.05 were considered significant.

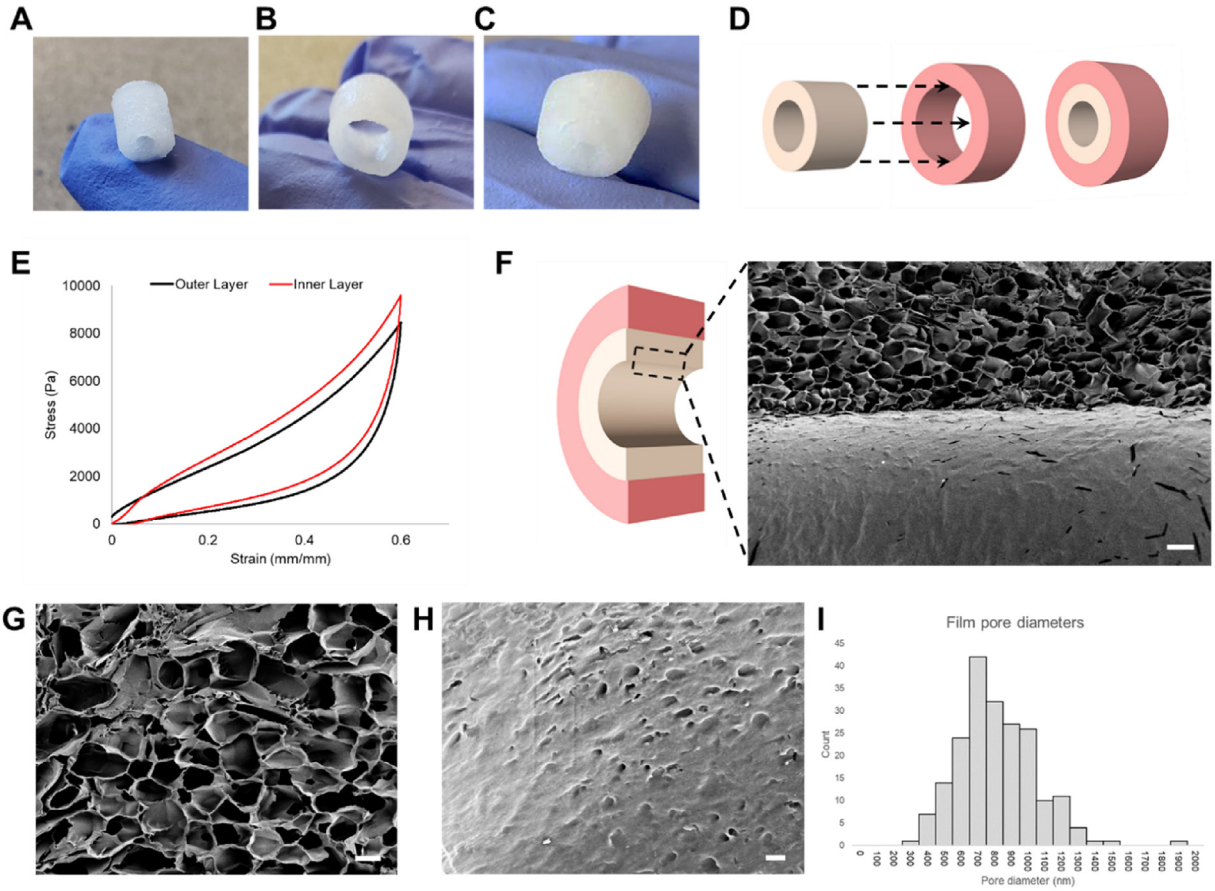

Fig. 1. Dimensions, stiffness, and porous film characterization of lyophilized silk matrices. 3D scaffold systems for intestinal tissue engineering were fabricated used silk fibroin. (A) Inner scaffolds are cylindrical constructs with an outer Ø of 6 mm, inner Ø of 2 mm, and length of 8 mm. (B) Outer scaffolds are wider cylindrical constructs capable of enclosing the inner scaffold with an outer Ø of 10 mm, inner Ø of 6 mm, and length of 8 mm. (C) Silk scaffold system with inner and outer scaffold combined (D) Dimensions of inner and outer scaffolds allow sliding of the inner scaffold into the hollow center of the outer scaffold. (E) Representative tress-strain curves of both outer and inner scaffolds (F) SEM cutaway of the interface between the film and sponge (scalebar: 200 μm) (G) Interconnected pores in the spongey bulk of scaffolds (scalebar: 100 μm) (H) Nanopores in the film (scalebar: 2 μm). (I) Aggregate diameters of nanopores (n = 201) averaged at 767 nm (s d. = 233 nm).

3. Results

3.1. Characterization of 3D silk sponges with a porous film for intestinal tissue engineering

The bilayer components were generated using silk fibroin isolated from *Bombyx mori* cocoons and processed following established protocols into lyophilized silk sponges with a hollow lumen space (diameter: 2 mm) [21,22,33]. A cylindrical inner scaffold was shaped using a 6 mm biopsy punch (inner diameter: 2 mm, outer diameter: 6 mm, length: 8 mm) and a hollow outer scaffold with a 10 mm biopsy punch (inner diameter: 6 mm, outer diameter: 10 mm, length: 8 mm) (Fig. 1A–C). The scaffold dimensions were designed to enable simple assembly of a bilayered silk sponge format in which the colonoid epithelial monolayer is cultured on the filmy surface of the inner layer and the macrophages are cultured throughout the outer layer (Fig. 1C and D). Compression testing of silk scaffolds yielded Young's moduli averaged at 18.16 kPa, within soft tissue moduli of 0.2–190 kPa [34] (Fig. 1E). Bulk properties of the lyophilized sponge have been previously characterized for pore size and degradation properties [35]. SEM imaging of the sponge microstructure showed a lumen surface with a film and a porous spongy bulk matrix directly underneath (Fig. 2F–H). The film consistently formed on the inner surface of silk scaffolds though the mechanism for its formation is unclear. We postulate that the interaction between the Teflon coated stainless-steel wire and the silk solution during the freezing process contributed to the film formation. Quantification of pore diameters on the film showed an average diameter of 767 nm (Fig. 1I).

3.2. Macrophage, colonoid, and tissue model cultivation

Human colonoids were cultured in Matrigel using established protocols prior to seeding in the tissue models [21,32,36] (Fig. 2A). Human monocytes were isolated from unpurified buffy coats using magnetic activated cell sorting and cryopreserved until needed (Fig. 2A). The colonoid epithelium of the tissue model was seeded by creating a single cells suspension of the colonoids and directly pipetting the suspension into the lumen space. Colonoid cells attached to the inner surface, forming a monolayer throughout the lumen surface (Fig. 2B). Monocytes were seeded in the bulk throughout the sponge of the outer layer and differentiated into a macrophage lineage prior to combining with the inner layer (Fig. 2B). The tissue model culture schedule consisted of 2 weeks of culture in High WNT media to ensure formation of a confluent colonoid epithelial layer within the tissue model, while preventing the colonoid monolayer from differentiating (Fig. 2C). The tissue model was then cultured in differentiation media for up to a week (Fig. 2C). A week was chosen as the terminal timepoint since colonoid monolayers seeded on transwell membranes remain functional for up to 7 days of differentiation (Supplementary Fig. S1). The outer layer with monocytes was differentiated independently into a macrophage lineage

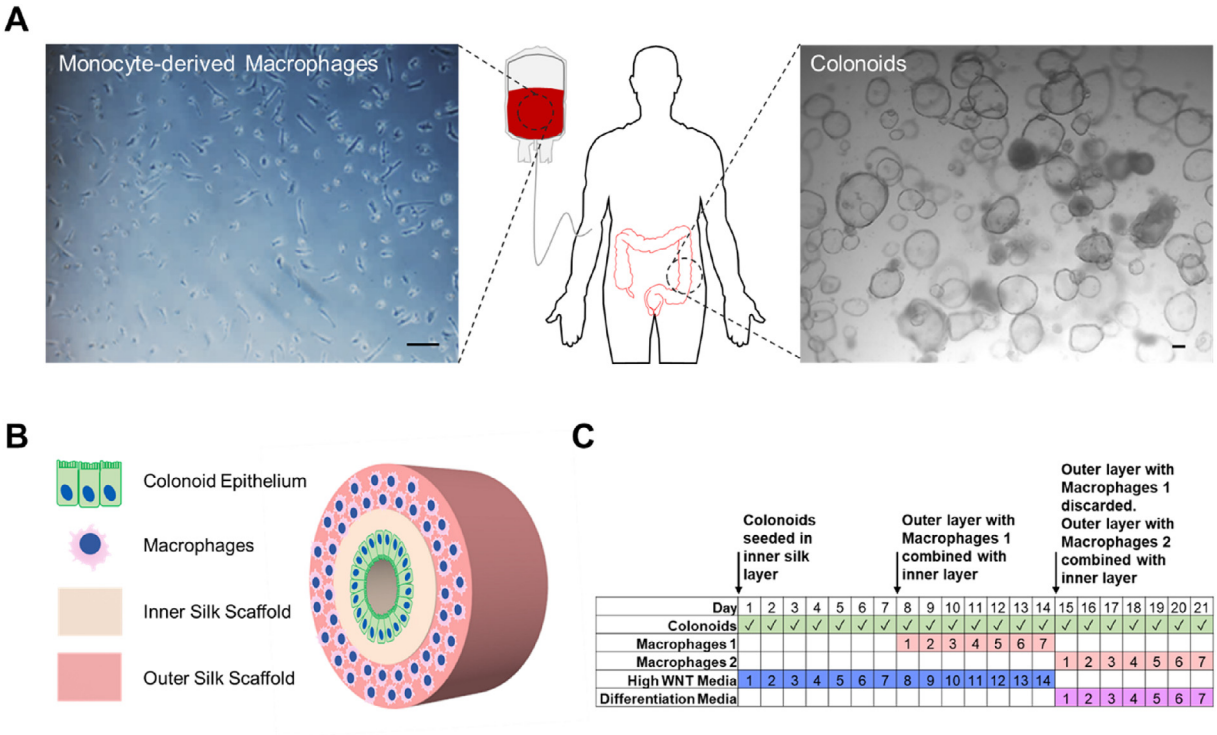

Fig. 2. Colonoid and macrophage cultivation scheme in the 3D bilayer system. **(A)** Human monocytes were isolated from whole blood and human colonoids from large intestine biopsies were cultured according to established protocols. **(B)** Cell suspensions of colonoids were seeded on the film surface on the inner silk scaffold and monocyte-derived macrophages were seeded throughout the porous outer silk scaffold. **(C)** The model is cultured for 3 weeks total with 2 weeks in High WNT media and 1 week in differentiation media. Colonoids are present in the model throughout the 3 week culture time. 2 sets of macrophages are added with the first set added after the first week of culture and the second set replacing the first set after the second week.

and added to the model 7 days prior to differentiation and again at the start of differentiation (Fig. 2C). The outer layer was replaced every 7 days due to up to 50% decreased metabolic activity of monocyte-derived macrophages in either high WNT or differentiation media by day 7 (Supplementary Fig. S2A).

3.3. Establishment of the tissue epithelial layer and macrophage outer layer

Fig. 3A outlines the tissue models constructed and analyzed to investigate the effects of macrophages and inflammatory cues on the colonoid epithelial layer. Staining for CD68, a pan-macrophage marker, and iNOS, an M1 polarized macrophage marker showed the presence of macrophages dispersed through the outer silk scaffold (Fig. 3B and C). iNOS expression was seen in macrophages regardless of culture in high WNT or differentiation media (Supplementary Fig. S2D). Control models were analyzed at day 3 and day 7 of differentiation to ensure lumen surface coverage by a single cell layer of polarized epithelial cells as seen *in* vivo (Fig. 3D). E-cadherin, a cell adhesion molecule selective for colonoid cells but not macrophages was used as an immunocytochemical marker for colonoids. At day 3, seeding of colonoids in the lumen resulted in the formation of an epithelial layer expressing E-cadherin (Fig. 3E). SEM imaging of the epithelial surface at day 7 confirmed a polarized epithelial surface with microvilli on the apical surface with defined borders between individual cells, indicating a functional and properly differentiated intestinal epithelium (Fig. 3F). Transverse sections of controls showed a fully confluent monolayer at day 3, replicating the intestinal monolayer found *in vivo* (Fig. 3G and H). A closer look at the epithelium showed individual cells arranged in a monolayer with e-cadherin expression between cells.

3.4. Macrophage infiltration into epithelium

Transverse histological sections of macrophage laden models at day 3 of differentiation (+MΦ, +MΦ + Inf) were examined for the presence of macrophage along the epithelium. Macrophages were identified by CD68 positive staining which does not stain intestinal epithelium. At 10X, $CD68^{+}$ staining was not readily observed (Fig. 4A), however 40X imaging of the epithelium showed $CD68^{+}$ cells along the basal side of the epithelium (Fig. 4A). Quantification of $CD68^{+}$ cells on histological sections showed a statistically significant difference between + MΦ and +MΦ + Inf models (Fig. 4B). Observation of $CD68^{+}$ cells along the epithelium suggests that macrophages in the outer layer of the model system were capable of movement through the silk-collagen matrix. The increased macrophage count in the +MΦ + Inf models over + MΦ was explained by increased levels chemotactic cues released by the inflamed epithelium (Fig. 6A).

3.5. Effects of macrophage co-culture and inflammatory cues on epithelial morphology and coverage

Lumen surfaces of each model group were stained with E-cadherin and MUC2 (Fig. 5A and B). E-cadherin staining showed clear differences in epithelial coverage at day 7 between inflamed and uninflamed groups (Fig. 5A). MUC2 staining which is indicative of goblet cells showed the presence of mucus producing goblet cells (Fig. 5B). To quantify epithelial coverage, transverse histological sections of the monolayer on the whole lumen were stained with E-cadherin (Fig. 5C). Epithelial coverage at day 7 evaluated via transverse sections reflect the epithelial coverage seen via lumen surface staining (Fig. 5A, C). Close examination of the epithelial layer showed differences in morphology between inflamed and uninflamed groups with a monolayer on uninflamed groups and a ball-like epithelial structure forming for inflamed groups (Fig. 5D). Alcian blue staining showed a thin layer of mucin on the epithelial cells in all groups (Fig. 5E). Epithelial height measurements reflected the morphological differences between groups observed in Fig. 5D with +MΦ + Inf displaying a higher epithelial height at day 7

A

Model Groups	Colonoids	Macrophages	Inflammation
Control	+	-	-
+Inf	+	-	+
+MΦ	+	+	-
+MΦ+Inf	+	+	+

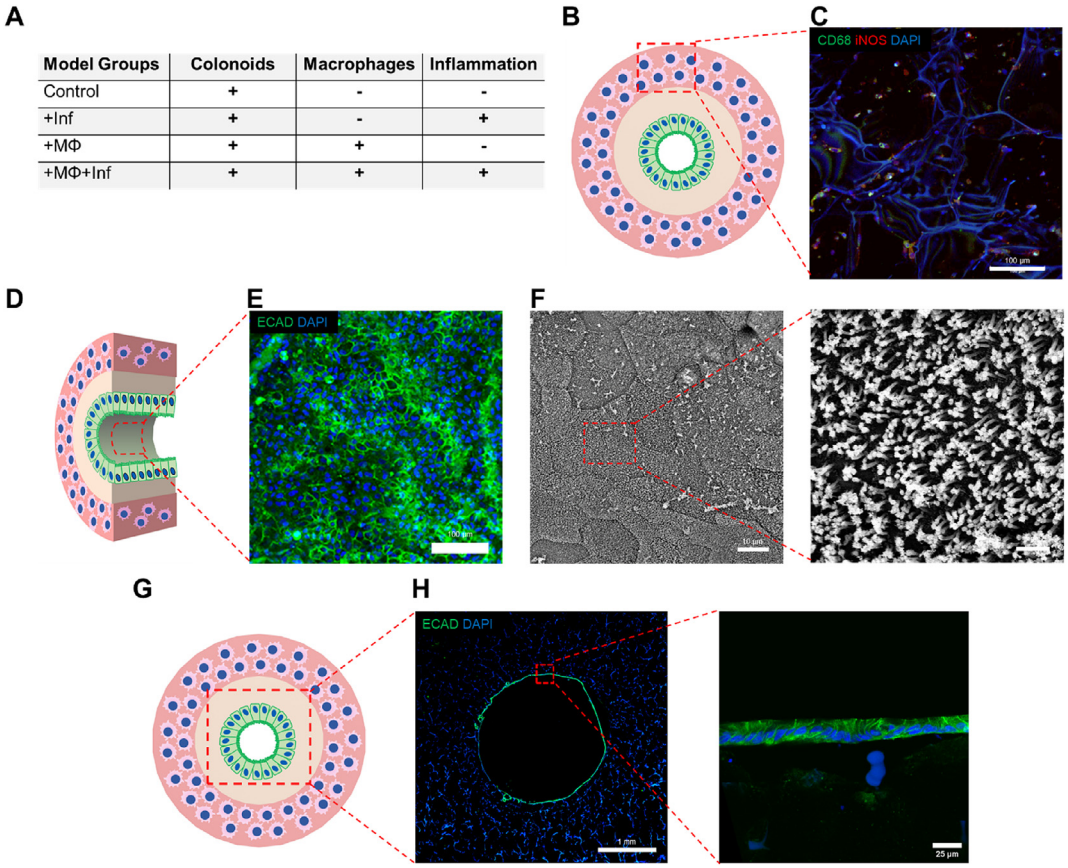

Fig. 3. Colonoid epithelial monolayer forms a polarized and confluent monolayer. (A) Table showing different group conditions for analyzing inflammation and macrophage contributions to model. All groups are seeded with colonoids. (B, C) The macrophage laden outer layer of the +MΦ+Inf group was imaged for CD68 and iNOS to show even distribution of macrophages throughout outer scaffold (scalebar: 100 μm). (D) The surface of the epithelial monolayer was imaged using immunofluorescence and SEM. (E) Colonoids seeded on inner scaffold lumen surface show consistent expression of e-cadherin at day 3 (scalebar: 100 μm) (F) SEM shows microvilli on the apical side of colonoids (scalebar: 10 μm and 1 μm respectively). (G) Transverse histological sections (thickness: 20 μm) of the 3D models were immunostained with e-cadherin to analyze epithelial coverage. (H) 3 days differentiated control models show a single cell layer of epithelium on the lumen surface. (scalebar: 1 mm and 25 μm).

compared to + MΦ at day 3 or 7 and control at Day 7 (Fig. 5F). This was explained by the overall higher epithelial heights seen in the ball-like structures in the inflamed groups. Lumen coverage was quantified based on the transverse sections at day 3 and day 7 (Fig. 5G). Epithelial coverage was highest for day 3 control tissue models followed by day 3 +MΦ models, though day 7 coverages between control and +MΦ were not statistically significant. Overall, the +MΦ group displayed a higher average coverage. +MΦ+Inf and +Inf groups at both days 3 and 7 had statistically significant coverage compared to the uninflamed groups. Though inflammation is known to play a role in goblet cell differentiation, the thickness of the mucus layers did not change between groups (Fig. 5H).

3.6. Effects of macrophages and inflammatory cues on cytokines secreted

The cytokine profiles of the tissue models were assayed using a cytokine array capable of measuring the presence of 80 cytokines and standardized by z-score to highlight relative differences of secreted cytokines between groups (Fig. 6A). To simplify cytokine array data, principle component analysis (PCA) was used to visualize compare overall cytokine profiles. The placement of PCA points in Fig. 6B showed that the cytokine profiles of each sample generally correspond to its treatment: control PCA placements were largely closest to each other as was the case with +MΦ, +Inf, and +MΦ+Inf samples (Fig. 6B). Hierarchical clusters were formed based on cytokine z-scores and used on the PCA plot to highlight distinct groups of samples (Fig. 6B). Four clusters were formed, mirroring the treatment groups in this study (Fig. 6B). To visualize how each individual cytokine contributed to PCA placements, a biplot showing the magnitude and direction of each cytokine's contribution to PCA placements was shown (Fig. 6C). To simplify the visualization, the 34 cytokines that were statistically significant between groups based on ANOVA were shown (Fig. 6C). Comparisons between groups for levels of cytokine secretions were tested for statistical significance via Tukey's Post Hoc test and all instances of reported higher secretion reflect statistical significance. Both macrophage groups + MΦ and +MΦ+Inf resulted in the higher secretions of ENA-78, G-CSF, GRO a/b/g, IL-10, IL-4, IL-5, MCP-3, MIF, and NAP-2 compared to control and +Inf. Proinflammatory cytokines IL-1β, IL-6, MCP-2, M-CSF, and MIP-1β were the highest secreted in +MΦ+Inf samples while + Inf showed similar levels of these proinflammatory cytokines as control. GCP-2 was the most highly secreted in the +MΦ group. Interestingly, control and +Inf which did not contain macrophages both had higher levels of IFN-γ, IL-13, IL-2, IL-8, TIMP-1, and VEGF-A than + MΦ or + MΦ+Inf groups. The control group had the highest secretion of GROα and MCP-1. All cytokines that were secreted in +Inf groups were secreted similar levels as control except for CXCL10. Both + Inf and +MΦ+Inf samples had similarly higher secretions of CXCL10 compared to control and +MΦ.

4. Discussion

The secondary layer of macrophages significantly contributed

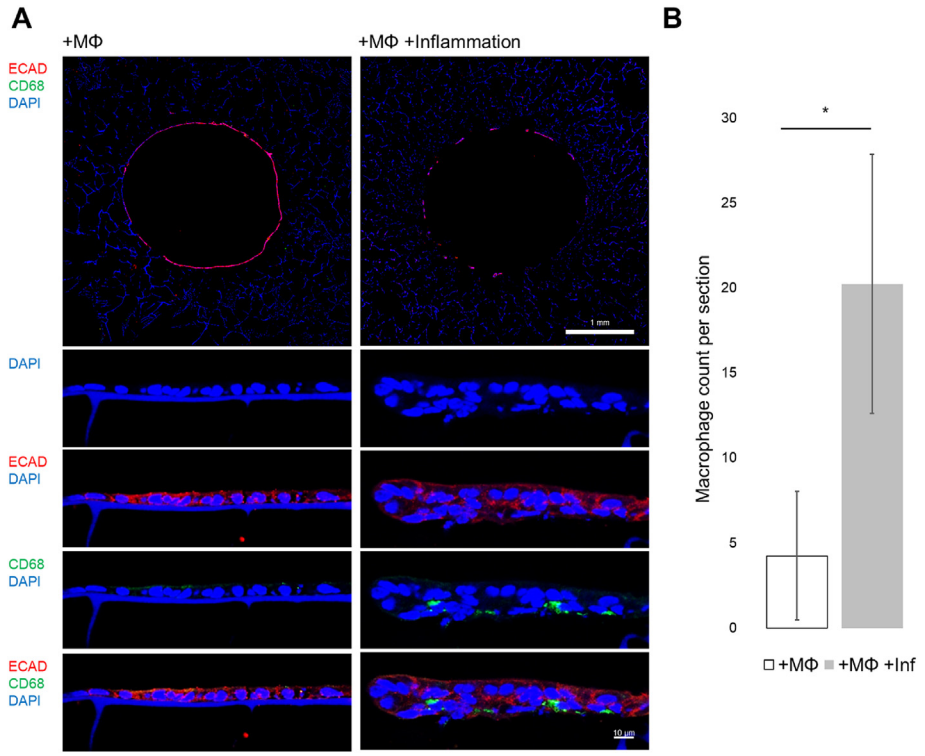

Fig. 4. Monocyte-derived macrophages infiltrating the epithelial monolayer under inflammation. (A) Transverse histological sections of models at day 3 show e-cadherin positive epithelial cells and little to no CD68 $^{+}$ cells at 10X (top scalebar 1 mm). Higher magnification images of the epithelium show CD68 $^{+}$ macrophages on the basal side of the epithelium of inflamed conditions (bottom scalebar 10 μm). (B) Quantification of CD68 $^{+}$ macrophage cells on transverse sections between + MO and +MO + Inflammation show statistical significance (n = 4) ($p < 0.05$).

towards inflammatory responses in a 3D tissue model of the large intestine epithelium by demonstrating leukocyte infiltration and pro-inflammatory cytokine secretion. These features have been reported in inflamed intestinal epithelial tissue from IBD patients and in serum samples of IBD patients with active inflammation [12,37–39]. This 3D tissue system, comprised of non-transformed human intestinal epithelia and macrophage immune compartments in a modular scaffold provides a useful 3D epithelial barrier model with utility in IBD and intestinal inflammation studies.

Biomaterial characterization and cell behavior suggested that the lyophilized silk sponge format was suitable as scaffolding material for engineering an intestinal epithelium with a 3D subepithelial space. *Bombyx mori* derived silk fibroin is a biocompatible scaffolding material which has been successfully used in intestinal epithelium systems and immune cell co-cultures [21–23,40]. Furthermore, silk is a well characterized biomaterial used in *in vivo* implants and tissue engineered systems due to its bio-inertness and versatility of material formats including films, hydrogels, and sponges [33]. In this study, we used lyophilized silk sponge matrices capable of forming a porous film layer for the cultivation of epithelial surfaces. SEM imaging of silk scaffolds used in this study showed a porous film capable of supporting a monolayer of epithelium for up to 21 days of culture (Fig. 1H and I 5A). The formation of monolayers supported the physiological relevance of colonoids as used in this study since the *in vivo* intestinal epithelium is also a single cell thick layer [18]. Moreover, SEM imaging of the epithelial monolayer at day 3 of differentiation showed dense microvilli formation on the apical side of the colonoid epithelium which is indicative of a functioning and differentiated epithelium [41]. Directly beneath the film structure was the spongey bulk, which presented a porous 3D matrix with interconnected pores which mimicked soft tissue stiffness (Fig. 1G,E) [34].

The presence of macrophages on the basal side of the epithelium suggested that the spongey silk construct was capable of supporting macrophage infiltration from the outer layer through the inner layer to the epithelium (Fig. 4A and B). Infiltration of macrophages towards an epithelium was a unique feature of this *in vitro* tissue model which is reflected in intestine tissue samples of IBD patients with active inflammation [12]. In Lissner et al., counts of CD68 positive cells in the tissue layer directly underneath the intestinal epithelium was significantly higher in samples of Crohn's disease than in normal intestine samples. Intestinal epithelial cells are key regulators of the intestinal immune system, releasing cytokines in response to inflammatory stimuli as well as under normal conditions [18,42]. The release of pro-inflammatory cytokines provides chemotactic cues which cause macrophages to migrate towards the inflamed epithelium.

Evaluation of the epithelial barrier in our tissue model demonstrated physiological responses to inflammation cues and macrophage co-culture. *In vitro* epithelial coverage was identified as a key metric based on increased epithelial cell death in inflamed IBD tissue compared to uninflamed tissue [43]. At both day 3 and 7, +Inf and MΦ+Inf tissue models presented lower epithelial coverage compared to uninflamed models, suggesting increased cell death, recapitulating inflamed tissue characteristics (Fig. 5G). Uninflamed models showed improved cell viability when compared to inflamed models (Fig. 5G). Furthermore, no significant differences in coverage were detected between control and +MΦ at day 7, suggesting cell death was unaffected by differences in co-culture conditions. Epithelial height was also measured since morphological changes can be observed in macrophage co-cultures and with inflammatory stimuli can be observed in transwell models [13]. Epithelial height was most pronounced in the +MΦ+Inf group, suggesting macrophages and inflammation contributed to differences in epithelial morphology (Fig. 5F). Histological sections of epithelia at day 7 reflected morphological changes with ball-like structures present in +MΦ+Inf groups instead of a monolayer as seen in the control or + MΦ groups (Fig. 5D). Mucus thickness was measured since cytokines such as IL-6, 10, and 33 are known to influence the secretion of mucin or the proliferation of intestinal goblet cells [44–46]. While the presence of a mucus layer was confirmed and its thickness measured, no significant differences were detected between the study groups, suggesting effects on mucus thickness may require a longer time to reflect *in vivo* mucus layer thickness changes observed *in vivo* (Fig. 5H).

Cytokines mediate inflammatory responses as well as immune functions under homeostasis, as a result systemic levels of specific

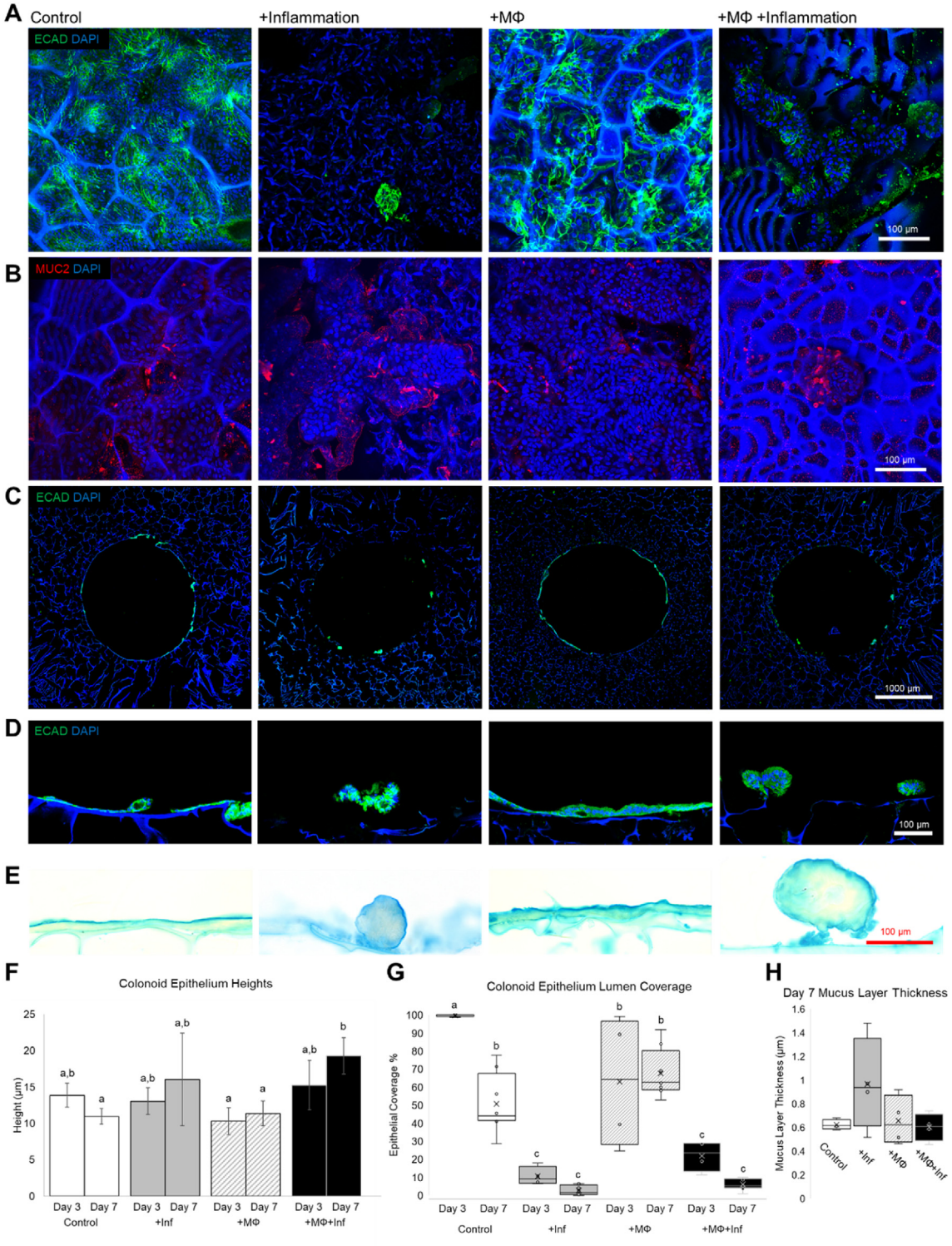

Fig. 5. Inflammatory cues and macrophages influence *in vitro* colonic epithelial coverage and morphology but not mucus thickness. (A) Lumen surface immunostaining for e-cadherin show differences in epithelial coverages between inflamed versus uninflamed groups at day 7 of differentiation (scalebar: 100 μm). (B) Luminal MUC2 staining shows positive staining on all groups indicating presence of goblet cells (scalebar: 100 μm). (C) Transverse histological sections of models at day 7 show variable epithelial coverages as seen by the e-cadherin immunostaining (scalebar 1 mm). (D) A closer look at the epithelia shows monolayers for uninflamed groups and ball like structures in inflamed groups (scalebar: 100 μm). (E) Alcian blue staining of transverse sections stains mucus layers (scalebar: 100 μm). (F) Quantification of epithelial heights between Day 3 and Day 7 for all groups show that the combination of macrophages and inflammatory cues results in morphologic differences ($n = 4–8$) ($p < 0.05$). (G) Epithelial coverage was quantified showing a decreased coverage in inflamed groups and over time ($n = 4–8$) ($p < 0.05$). (H) Mucus layer thickness at day 7 showed no significant changes between groups ($n = 4–8$) ($p < 0.05$). . (For interpretation of the references to colour in this figure legend, the reader is referred to the Web version of this article.)

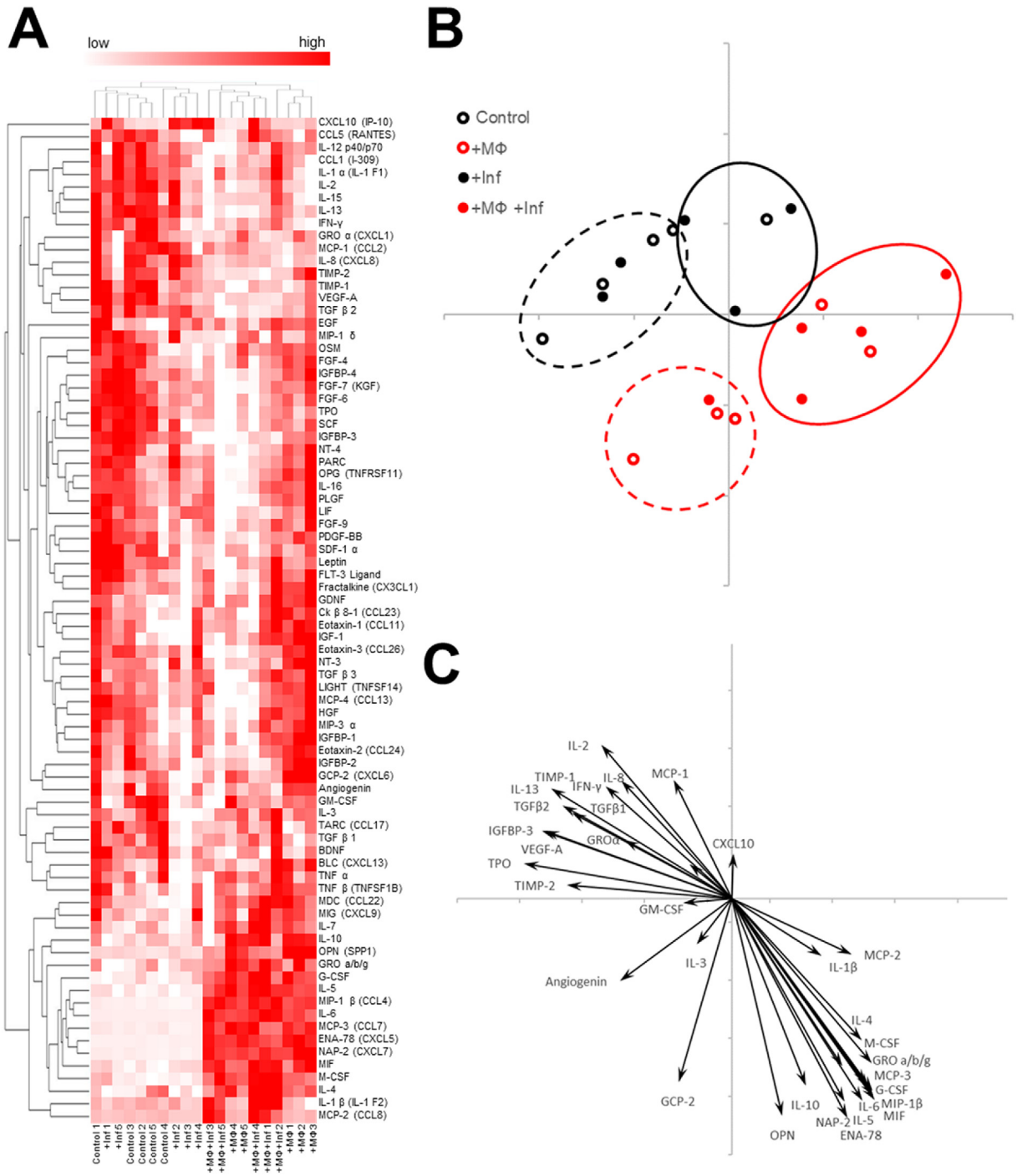

Fig. 6. Addition of macrophages and inflammatory cues each contribute to unique cytokine profiles. (A) 80 cytokines were assayed in the model media at day 3 of differentiation. Cytokine blot intensities were standardized by z-score and reported in a heat map. Heat scores for each individual sample were represented with red denoting higher relative concentration. (n = 5). (B) Principal component analysis was used to interpret the cytokine profiles of each sample. Hierarchical clustering of the cytokine data was used to group each cytokine profile. (C) Biplot of statistically significant cytokine z-scores based on ANOVA shows contributions of cytokines to principal component analysis placements ($p < 0.05$). . (For interpretation of the references to colour in this figure legend, the reader is referred to the Web version of this article.)

cytokines differ between patients with IBD and healthy patients [38,48]. Our tissue models also reflected differences in secreted cytokines with each study group presenting unique cytokine profiles, however, the addition of macrophages contributed to a more physiologically relevant cytokine profile in both the uninflamed and inflamed cases (Fig. 5B and C). Statistical significance of cytokine levels between groups was tested via ANOVA followed by Tukey's Post Hoc test and all instances of reported higher secretion reflect statistical significance. Control and +Inf groups which did not have macrophages had higher levels (compared to + MΦ and +MΦ+Inf) of pleiotropic cytokine IL-2 [49], extracellular remodeling cytokine TIMP-1 [50], and angiogenic cytokines IL-8 and VEGF-A [51,52]. Interestingly, the control group also expressed the highest levels of proinflammatory protein MCP-1 in addition to angiogenic cytokine GROα, a CXC chemokine which binds to IL8RB and mediates the same angiogenic activity as IL-8 [51,53]. The effects of inflammatory cues on the colonoid epithelium without

macrophages showed elevated secretion of only CXCL10, a pro-inflammatory cytokine that is elevated in IBD patient sera [38]. However, levels of CXCL10 were statistically significant and similarly high in the +MΦ+Inf group compared to control (Fig. 6A, C). Overall, the groups without macrophages (control and +Inf) displayed statistically significant higher expression of cytokines mediating angiogenesis which was not reflected in the groups with macrophages (+MΦ and +MΦ+Inf). Elevated cytokines as confirmed by statistical significance via Tukey's Post Hoc test in both + MΦ and +MΦ+Inf models included pro-inflammatory cytokine MIF [54], anti-inflammatory cytokine IL-10 and IL-4 [55,56], monocyte chemotactic cytokines MCP-3 and GRO a/b/g [57–59], neutrophil chemotactic cytokine ENA-78/CXCL5 and NAP-2 [57,60], and granulocyte and neutrophil mediating cytokine G-CSF [61]. Pro-inflammatory cytokines with higher expression in patients biopsy samples or sera with active IBD compared to healthy patients including IL-1β [38], IL-6 [48,62], MCP-2 [63], and MIP-1β [63] were statistically significant and highly expressed in the +MΦ+Inf samples compared to all other groups. Elevated secretion of multiple pro-inflammatory cytokines associated with active IBD in +MΦ+Inf samples but not in +Inf samples suggested that the macrophage laden outer layer enhanced the biochemical response and as a result, the physiologic relevance of the 3D colonoid model.

5. Conclusions

Our *in vitro* model displays phenotypic responses to inflammation through epithelial barrier disruption, macrophage migration, and the secretion of cytokines associated with IBD. Culture of the colonoid monolayers on the silk scaffolds resulted in a polarized epithelium displaying microvilli on the apical surface with infiltration of macrophages from the outer layer to the basal surface of the epithelium. Our results confirmed a need for an immune cell component in intestinal epithelial models and demonstrates the utility of this tissue system consisting of colonoids and macrophages, versus an epithelium only model, in evaluating the effects of inflammatory cues on epithelial morphological features and biochemical composition. Further development of the *in vitro* tissue model system to enable longer-term cultures for the study of chronic effects of inflammation are suggested based on the responses reported here. As a tissue platform for studying epithelial-immune reactions against inflammatory cues, this *in vitro* model may be used for studying the response of a human intestinal epithelium and immune system against acute pathogenic insults and modulation of active inflammation in IBD.

Funding sources

Support from the NIH (P41EB002520, U19-AI131126) and the Air Force Office of Scientific Research, National Defense Science and Engineering Graduate (NDSEG) Fellowship is greatly appreciated. This work was also supported by the NIH Research Infrastructure grant NIH S10 OD021624. Scanning electron microscopy was performed at the Center for Nanoscale Systems (CNS), a member of the National Nanotechnology Infrastructure Network (NNIN). CNS is part of the Faculty of Arts and Sciences at Harvard University.

Appendix A. Supplementary data

Supplementary data to this article can be found online at https://doi.org/10.1016/j.biomaterials.2019.119517.

References

[1] R. Sender, S. Fuchs, R. Milo, Revised estimates for the number of human and bacteria cells in the body, PLoS Biol. 14 (8) (2016) e1002533.
[2] E. Thursby, N. Juge, Introduction to the human gut microbiota, Biochem. J. 474 (11) (2017) 1823–1836.
[3] A.M. Mowat, W.W. Agace, Regional specialization within the intestinal immune system, Nat. Rev. Immunol. 14 (2014) 667.
[4] L.C. Davies, S.J. Jenkins, J.E. Allen, P.R. Taylor, Tissue-resident macrophages, Nat. Immunol. 14 (10) (2013) 986–995.
[5] A.A. Kühl, U. Erben, L.I. Kredel, B. Siegmund, Diversity of intestinal macrophages in inflammatory bowel diseases, Front. Immunol. 6 (2015) 613-613.
[6] A.M. Mowat, C.L. Scott, C.C. Bain, Barrier-tissue macrophages: functional adaptation to environmental challenges, Nat. Med. 23 (2017) 1258.
[7] P.D. Smith, L.E. Smythies, R. Shen, T. Greenwell-Wild, M. Gliozzi, S.M. Wahl, Intestinal macrophages and response to microbial encroachment, Mucosal Immunol. 4 (2010) 31.
[8] S.H. Lee, P.M. Starkey, S. Gordon, Quantitative analysis of total macrophage content in adult mouse tissues. Immunochemical studies with monoclonal antibody F4/80, J. Exp. Med. 161 (3) (1985) 475–489.
[9] A. Lahiri, C. Abraham, Activation of pattern recognition receptors up-regulates metallothioneins, thereby increasing intracellular accumulation of zinc, autophagy, and bacterial clearance by macrophages, Gastroenterology 147 (4) (2014) 835–846.
[10] F. D'Angelo, E. Bernasconi, M. Schäfer, M. Moyat, P. Michetti, M.H. Maillard, D. Velin, Macrophages promote epithelial repair through hepatocyte growth factor secretion, Clin. Exp. Immunol. 174 (1) (2013) 60–72.
[11] D. Ortiz-Masiá, J. Cosín-Roger, S. Calatayud, C. Hernández, R. Alós, J. Hinojosa, N. Apostolova, A. Alvarez, M.D. Barrachina, Hypoxic macrophages impair autophagy in epithelial cells through Wnt1: relevance in IBD, Mucosal Immunol. 7 (2013) 929.
[12] D. Lissner, M. Schumann, A. Batra, L.-I. Kredel, A.A. Kühl, U. Erben, C. May, J.-D. Schulzke, B. Siegmund, Monocyte and M1 macrophage-induced barrier defect contributes to chronic intestinal inflammation in IBD, Inflamm. Bowel Dis. 21 (6) (2015) 1297–1305.
[13] G. Noel, N.W. Baetz, J.F. Staab, M. Donowitz, O. Kovbasnjuk, M.F. Pasetti, N.C. Zachos, A primary human macrophage-enteroid co-culture model to investigate mucosal gut physiology and host-pathogen interactions, Sci. Rep. 7 (2017) 45270.
[14] H.J. Kim, H. Li, J.J. Collins, D.E. Ingber, Contributions of microbiome and mechanical deformation to intestinal bacterial overgrowth and inflammation in a human gut-on-a-chip, Proc. Natl. Acad. Sci. 113 (1) (2016) E7.
[15] R.H. Dosh, N. Jordan-Mahy, C. Sammon, C.L. Le Maitre, Long-term in vitro 3D hydrogel co-culture model of inflammatory bowel disease, Sci. Rep. 9 (1) (2019) 1812.
[16] A. Sehgal, D.S. Donaldson, C. Pridans, K.A. Sauter, D.A. Hume, N.A. Mabbott, The role of CSF1R-dependent macrophages in control of the intestinal stem-cell niche, Nat. Commun. 9 (1) (2018) 1272.
[17] T. Sato, D.E. Stange, M. Ferrante, R.G.J. Vries, J.H. van Es, S. van den Brink, W.J. van Houdt, A. Pronk, J. van Gorp, P.D. Siersema, H. Clevers, Long-term expansion of epithelial organoids from human colon, adenoma, adenocarcinoma, and barrett's epithelium, Gastroenterology 141 (5) (2011) 1762–1772.
[18] L.W. Peterson, D. Artis, Intestinal epithelial cells: regulators of barrier function and immune homeostasis, Nat. Rev. Immunol. 14 (2014) 141.
[19] C.R. Weber, J.R. Turner, Inflammatory bowel disease: is it really just another break in the wall? Gut 56 (1) (2007) 6–8.
[20] C. Andrews, M.H. McLean, S.K. Durum, Cytokine tuning of intestinal epithelial function, Front. Immunol. 9 (2018) 1270-1270.
[21] Y. Chen, W. Zhou, T. Roh, M.K. Estes, D.L. Kaplan, In vitro enteroid-derived three-dimensional tissue model of human small intestinal epithelium with innate immune responses, PLoS One 12 (11) (2017) e0187880.
[22] Y. Chen, Y. Lin, Q. Wang, J. Rnjak-Kovacina, C. Li, R.R. Isberg, C.A. Kumamoto, J. Mecsas, D. Kaplan, Robust Bioengineered 3D Functional Human Intestinal Epithelium, (2015).
[23] W. Zhou, Y. Chen, T. Roh, Y. Lin, S. Ling, S. Zhao, J.D. Lin, N. Khalil, D.M. Cairns, E. Manousiouthakis, M. Tse, D.L. Kaplan, Multifunctional bioreactor system for human intestine tissues, ACS Biomater. Sci. Eng. 4 (1) (2018) 231–239.
[24] J. Barthes, C. Dollinger, C.B. Muller, U. Liivas, A. Dupret-Bories, H. Knopf-Marques, N.E. Vrana, Immune assisted tissue engineering via incorporation of macrophages in cell-laden hydrogels under cytokine stimulation, Front. Bioeng. Biotechnol. 6 (2018) 108-108.
[25] E. Dohle, I. Bischoff, T. Bose, A. Marsano, A. Banfi, R.E. Unger, C.J. Kirkpatrick, Macrophage-mediated angiogenic activation of outgrowth endothelial cells in co-culture with primary osteoblasts, Eur. Cells Mater. 27 (2014) 149–164 discussion 164-5.
[26] C. Dollinger, S. Ciftci, H. Knopf-Marques, R. Guner, A.M. Ghaemmaghami, C. Debry, J. Barthes, N.E. Vrana, Incorporation of resident macrophages in engineered tissues: multiple cell type response to microenvironment controlled macrophage-laden gelatine hydrogels, J. Tissue Eng. Regenerat. Med. 12 (2) (2018) 330–340.
[27] C.C. Bain, A. Bravo-Blas, C.L. Scott, E. Gomez Perdiguero, F. Geissmann, S. Henri, B. Malissen, L.C. Osborne, D. Artis, A.M. Mowat, Constant replenishment from circulating monocytes maintains the macrophage pool in the intestine of adult mice, Nat. Immunol. 15 (2014) 929.
[28] S. Thiesen, S. Janciauskiene, H. Uronen-Hansson, W. Agace, C.-M. Högerkorp, P. Spee, K. Håkansson, O. Grip, CD14hiHLA-DRdim macrophages, with a resemblance to classical blood monocytes, dominate inflamed mucosa in Crohn's disease, J. Leukoc. Biol. 95 (3) (2014) 531–541.
[29] J.R. Grainger, E.A. Wohlfert, I.J. Fuss, N. Bouladoux, M.H. Askenase, F. Legrand, L.Y. Koo, J.M. Brenchley, I.D.C. Fraser, Y. Belkaid, Inflammatory monocytes regulate pathologic responses to commensals during acute gastrointestinal infection, Nat. Med. 19 (6) (2013) 713–721.
[30] K. Asano, N. Takahashi, M. Ushiki, M. Monya, F. Aihara, E. Kuboki, S. Moriyama, M. Iida, H. Kitamura, C.-H. Qiu, T. Watanabe, M. Tanaka, Intestinal CD169(+)

macrophages initiate mucosal inflammation by secreting CCL8 that recruits inflammatory monocytes, Nat. Commun. 6 (2015) 7802-7802.
[31] C.C. Bain, A.M. Mowat, Macrophages in intestinal homeostasis and inflammation, Immunol. Rev. 260 (1) (2014) 102–117.
[32] J. In, J. Foulke-Abel, N.C. Zachos, A.-M. Hansen, J.B. Kaper, H.D. Bernstein, M. Halushka, S. Blutt, M.K. Estes, M. Donowitz, O. Kovbasnjuk, Enterohemorrhagic Escherichia coli reduce mucus and intermicrovillar bridges in human stem cell-derived colonoids, Cell. Mol. Gastroenterol. Hepatol. 2 (1) (2015) 48–62 e3.
[33] D.N. Rockwood, R.C. Preda, T. Yücel, X. Wang, M.L. Lovett, D.L. Kaplan, Materials fabrication from Bombyx mori silk fibroin, Nat. Protoc. 6 (10) (2011) 1612–1631.
[34] R. Feiner, T. Dvir, Tissue–electronics interfaces: from implantable devices to engineered tissues, Nat. Rev. Mater. 3 (2017) 17076.
[35] J. Rnjak-Kovacina, L.S. Wray, K.A. Burke, T. Torregrosa, J.M. Golinski, W. Huang, D.L. Kaplan, Lyophilized silk sponges: a versatile biomaterial platform for soft tissue engineering, ACS Biomater. Sci. Eng. 1 (4) (2015) 260–270.
[36] T. Sato, R.G. Vries, H.J. Snippert, M. van de Wetering, N. Barker, D.E. Stange, J.H. van Es, A. Abo, P. Kujala, P.J. Peters, H. Clevers, Single Lgr5 stem cells build crypt–villus structures in vitro without a mesenchymal niche, Nature 459 (2009) 262.
[37] J.M. Blander, Death in the intestinal epithelium-basic biology and implications for inflammatory bowel disease, FEBS J. 283 (14) (2016) 2720–2730.
[38] U.P. Singh, N.P. Singh, E.A. Murphy, R.L. Price, R. Fayad, M. Nagarkatti, P.S. Nagarkatti, Chemokine and cytokine levels in inflammatory bowel disease patients, Cytokine 77 (2016) 44–49.
[39] M.F. Neurath, Cytokines in inflammatory bowel disease, Nat. Rev. Immunol. 14 (2014) 329.
[40] S.E.L. Vidal, K.A. Tamamoto, H. Nguyen, R.D. Abbott, D.M. Cairns, D.L. Kaplan, 3D biomaterial matrix to support long term, full thickness, immuno-competent human skin equivalents with nervous system components, Biomaterials 198 (2019) 194–203.
[41] S.W. Crawley, M.S. Mooseker, M.J. Tyska, Shaping the intestinal brush border, J. Cell Biol. 207 (4) (2014) 441.
[42] J.C. Onyiah, S.P. Colgan, Cytokine responses and epithelial function in the intestinal mucosa, Cell. Mol. Life Sci. 73 (22) (2016) 4203–4212.
[43] A. Di Sabatino, R. Ciccocioppo, O. Luinetti, L. Ricevuti, R. Morera, M.G. Cifone, E. Solcia, G.R. Corazza, Increased enterocyte apoptosis in inflamed areas of Crohn's disease, Dis. Colon Rectum 46 (11) (2003) 1498–1507.
[44] S.Z. Hasnain, S. Tauro, I. Das, H. Tong, A.C.H. Chen, P.L. Jeffery, V. McDonald, T.H. Florin, M.A. McGuckin, IL-10 promotes production of intestinal mucus by suppressing protein misfolding and endoplasmic reticulum stress in goblet cells, Gastroenterology 144 (2) (2013) 357–368 e9.
[45] K.A. Kuhn, H.M. Schulz, E.H. Regner, E.L. Severs, J.D. Hendrickson, G. Mehta, A.K. Whitney, D. Ir, N. Ohri, C.E. Robertson, D.N. Frank, E.L. Campbell, S.P. Colgan, Bacteroidales recruit IL-6-producing intraepithelial lymphocytes in the colon to promote barrier integrity, Mucosal Immunol. 11 (2) (2018) 357–368.
[46] A. Waddell, J.E. Vallance, P.D. Moore, A.T. Hummel, D. Wu, S.K. Shanmukhappa, L. Fei, M.K. Washington, P. Minar, L.A. Coburn, S. Nakae, K.T. Wilson, L.A. Denson, S.P. Hogan, M.J. Rosen, IL-33 signaling protects from murine oxazolone colitis by supporting intestinal epithelial function, Inflamm. Bowel Dis. 21 (12) (2015) 2737–2746.
[48] J. Mudter, M.F. Neurath, Il-6 signaling in inflammatory bowel disease: pathophysiological role and clinical relevance, Inflamm. Bowel Dis. 13 (8) (2007) 1016–1023.
[49] N. Arenas-Ramirez, J. Woytschak, O. Boyman, Interleukin-2: biology, design and application, Trends Immunol. 36 (12) (2015) 763–777.
[50] K. Brew, D. Dinakarpandian, H. Nagase, Tissue inhibitors of metalloproteinases: evolution, structure and function11Dedicated to Professor H. Neurath on the occasion of his 90th birthday, Biochim. Biophys. Acta Protein Struct. Mol. Enzymol. 1477 (1) (2000) 267–283.
[51] K. Inoue, J.W. Slaton, B.Y. Eve, S.J. Kim, P. Perrotte, M.D. Balbay, S. Yano, M. Bar-Eli, R. Radinsky, C.A. Pettaway, C.P.N. Dinney, Interleukin 8 expression regulates tumorigenicity and metastases in androgen-independent prostate cancer, Clin. Cancer Res. 6 (5) (2000) 2104.
[52] A. Hoeben, B. Landuyt, M.S. Highley, H. Wildiers, A.T. Van Oosterom, E.A. De Bruijn, Vascular endothelial growth factor and angiogenesis, Pharmacol. Rev. 56 (4) (2004) 549.
[53] M. Miyake, S. Goodison, V. Urquidi, E. Gomes Giacoia, C.J. Rosser, Expression of CXCL1 in human endothelial cells induces angiogenesis through the CXCR2 receptor and the ERK1/2 and EGF pathways, Lab. Investig. 93 (2013) 768.
[54] T. Calandra, T. Roger, Macrophage migration inhibitory factor: a regulator of innate immunity, Nat. Rev. Immunol. 3 (10) (2003) 791–800.
[55] P. Krause, V. Morris, J.A. Greenbaum, Y. Park, U. Bjoerheden, Z. Mikulski, T. Muffley, J.-W. Shui, G. Kim, H. Cheroutre, Y.-C. Liu, B. Peters, M. Kronenberg, M. Murai, IL-10-producing intestinal macrophages prevent excessive antibacterial innate immunity by limiting IL-23 synthesis, Nat. Commun. 6 (2015) 7055-7055.
[56] P.H. Hart, G.F. Vitti, D.R. Burgess, G.A. Whitty, D.S. Piccoli, J.A. Hamilton, Potential antiinflammatory effects of interleukin 4: suppression of human monocyte tumor necrosis factor alpha, interleukin 1, and prostaglandin E2, Proc. Natl. Acad. Sci. U.S.A. vol. 86, 1989, pp. 3803–3807 10.
[57] S.K. Ahuja, P.M. Murphy, The CXC chemokines growth-regulated oncogene (GRO) α, GROβ, GROγ, neutrophil-activating peptide-2, and epithelial cell-derived neutrophil-activating peptide-78 are potent agonists for the type B, but not the type A, human interleukin-8 receptor, J. Biol. Chem. 271 (34) (1996) 20545–20550.
[58] T. Persson, N. Monsef, P. Andersson, A. Bjartell, J. Malm, J. Calafat, A. Egesten, Expression of the neutrophil-activating CXC chemokine ENA-78/CXCL5 by human eosinophils, Clin. Exp. Allergy 33 (4) (2003) 531–537.
[59] W. Xuan, Q. Qu, B. Zheng, S. Xiong, G.-H. Fan, The chemotaxis of M1 and M2 macrophages is regulated by different chemokines, J. Leukoc. Biol. 97 (1) (2015) 61–69.
[60] A. Walz, B. Dewald, V. von Tscharner, M. Baggiolini, Effects of the neutrophil-activating peptide NAP-2, platelet basic protein, connective tissue-activating peptide III and platelet factor 4 on human neutrophils, J. Exp. Med. 170 (5) (1989) 1745–1750.
[61] A.W. Roberts, G. CSF, A key regulator of neutrophil production, but that's not all!, Growth Factors 23 (1) (2005) 33–41.
[62] Y. Suzuki, H. Saito, J. Kasanuki, T. Kishimoto, Y. Tamura, S. Yoshida, Significant increase of interleukin 6 production in blood mononuclear leukocytes obtained from patients with active imflammatory bowel disease, Life Sci. 47 (24) (1990) 2193–2197.
[63] C. Banks, A. Bateman, R. Payne, P. Johnson, N. Sheron, Chemokine expression in IBD. Mucosal chemokine expression is unselectively increased in both ulcerative colitis and Crohn's disease, J. Pathol. 199 (1) (2003) 28–35.